

Sources of acoustic resonance generated by flow around a long rectangular plate in a duct

B.T. Tan, M.C. Thompson*, K. Hourigan

*FLAIR—Fluids Laboratory for Aeronautical and Industrial Research, Department of Mechanical Engineering, Monash University,
P.O. Box 31, Clayton 3800, Victoria, Australia*

Received 13 February 2003; accepted 12 August 2003

Abstract

This paper describes a numerical investigation of the acoustic resonance occurring at specific flow speeds when a long two-dimensional rectangular plate is placed on the centre-line of a duct. The flow Mach number is sufficiently small that the flow and acoustic fields can be modelled separately; however, the effect of the acoustic field in modifying the flow field is accounted for and, in turn, the flow field solution determines the time-dependent source distribution for the acoustic model. This allows the range of flow speeds, or equivalently the associated Strouhal numbers, where resonance is possible to be predicted. It is shown that the Strouhal number based on plate chord (or length) displays a stepping behaviour as the plate length is increased. The main source or sink region where energy is transferred between the acoustic and flow fields is shown to be immediately downstream of the trailing edge of the plate. Visualizations of the numerical solution show that the timing when the vortices enter this region relative to the phase of the acoustic cycle is crucial in determining if resonance can occur and is the cause of the observed stepwise increase. Comparison is made with previous physical experiments.

© 2003 Elsevier Ltd. All rights reserved.

1. Introduction

In this paper, the flow past a long two-dimensional rectangular plate (or cylinder) placed on the centre-line of duct is studied, together with the possibly resonant flow-induced acoustic field associated with this flow. For the cases considered, the plate is long relative to its thickness. Besides being a coupled flow/acoustic problem of intrinsic interest, it has associated industrial applications in the fields of wind engineering, turbomachinery and heat transfer. For example, turbomachinery devices can undergo severe flow-induced resonant interactions between blades rows that can cause long-term fatigue or even catastrophic structural failure.

There have been a number of different approaches to coupled acoustic flow problems presented in the literature. Conceptually, the most obvious way to treat such problems is using direct compressible flow simulations such as in the recent study of the acoustics associated with flow past a circular cylinder at low Reynolds numbers by Inoue and Hatakeyama (2002). This approach is extremely computationally expensive, especially at low Mach numbers, and it is still computationally prohibitive to calculate more than a few cycles. Another approach is to decouple the flow and acoustic problem, solving the flow directly and using an acoustic analogy (e.g., Lighthill, 1952; Curle, 1955) to predict the acoustic response. This is considerably cheaper computationally, but is restricted to low Mach numbers, since the source region needs to be compact relative to the acoustic wavelength. This approach has been recently applied to the flow-acoustic problem of flow past a cylinder by Tam and Hardin (1997). A third approach is known as acoustic/

*Corresponding author. Tel.: +61-3-9905-9645; fax: +61-3-9905-9639.
E-mail address: mark.thompson@eng.monash.edu.au (M.C. Thompson).

viscous splitting (Hardin and Pope, 1994). This method again splits the problem into flow and acoustic subproblems. It solves for the incompressible mean flow and then uses this to solve perturbation equations for the compressible component but without invoking an acoustic analogy. In the far field this compressible component is equivalent to the acoustic field. Recently, this method also has been applied to flow past a cylinder at low Reynolds numbers by Shen and Sorensen (1999). Review articles describing various approaches and applications are given in Tam (1995), Lele (1997), and Moin and Mahesh (1998). For the problem considered in this paper, these approaches are either too computationally expensive, or do not directly incorporate the required flow-acoustic feedback mechanism necessary to study the resonance problem. For a plate in a duct the resonance builds up over many shedding/acoustic cycles, as the sound produced by the vortex–body interactions slowly builds up the resonant field, which in turn modifies the flow field until resonance is established. An attack using a direct compressible flow simulation would therefore be prohibitive and would not be suitable for the parameter study undertaken with the current approach discussed below. This is also true for the methods based on the acoustic analogies and acoustic/viscous splitting even if they could be extended to include the feedback mechanism.

There have been numerous studies on the flow around long plates in the absence of external influences such as duct walls or an applied perturbation field. It has been found in both experimental (Nakamura et al., 1991; Naudascher and Wang, 1993), and numerical studies (Nakayama et al., 1993; Ohya et al., 1992) that shedding from the upper and lower faces of the plate are out of phase and lock to a single frequency. The Strouhal number, $St_c = fc/U_\infty$, based on chord c (where f is the frequency and U_∞ the upstream flow speed) shows a stepwise increase with increasing aspect ratio. Phase measurements along the plate show there are discrete vortices being shed from the leading edge of the plate which convect downstream. The steps in St_c with aspect ratio (c/t , with t the plate thickness) can be associated with the constancy in the number of vortex structures distributed along the upper or lower surface of the plate over each aspect ratio range. Also observed is that the phase at which the vortices pass the trailing edge relative to the leading-edge shedding is approximately constant. These observations led to the hypothesis that a feedback loop was established. The main elements of the feedback loop comprised vortices shed from the leading edge that later passed the trailing edge generating a pressure pulse, which in turn propagated upstream to lock further leading-edge shedding. More recently, Hourigan et al. (2001) have shown the presence of strong vortices forming at the trailing edge between the passing of leading-edge vortices and it has been proposed that the trailing-edge shedding plays a significant role in controlling the details of the feedback loop.

The hypothesized feedback loop has been previously described as an impinging leading-edge vortex instability (Naudascher and Wang, 1993; Mills et al., 2002). This mechanism is relatively weak and is able to lock the flow only at low Reynolds numbers ($Re = U_\infty t/\nu < 2000$, with ν the kinematic viscosity) and for limited aspect ratios ($c/t < 12$) (Nakamura et al., 1991). Note the Reynolds number is based on plate thickness.

At higher Reynolds numbers ($Re \approx 12000$) experiments have shown that, although the feedback mechanism no longer occurs naturally, the same receptivity continues to exist and can be observed with only low levels of cross-flow sinusoidal forcing (Mills et al., 2002, 2003). In particular, measurements of base pressure show the frequency at which the strongest base suction occurs increases in a stepwise fashion similar to that observed for the natural shedding case. Simulations, although at much lower Reynolds number ($Re = 400$), also show this behaviour (Tan et al., 1998a–c). In this case, instead of the pressure pulse from the trailing edge, it is the external perturbation that directly locks the leading-edge shedding. While the leading-edge shedding is phase-locked with the forcing, the simulations have shown that the phase of these vortices passing the trailing edge is a function of the aspect ratio and the forcing frequency. This is consistent with the convective velocity along the plate being relatively independent of these parameters. As in the unforced case, the phase of the shedding at the trailing edge relative to the leading edge is similar at all aspect ratios where the maximum response in base suction is observed. In fact, when the maximum response is observed, the relative phase between the shedding at the leading and trailing edge is similar to the natural shedding case.

The same Strouhal number stepping is also observed when a plate is placed in a duct. The sketch in Fig. 1 shows the set-up. The plate is placed centrally with the long axis parallel to the mean flow direction. Although it is possible to excite numerous acoustic modes in the duct, this study is concerned with the first β -mode (as defined in Parker, 1966). This consists of a single standing wave in the cross-flow direction. This field has an acoustic particle velocity anti-node at the centre of the duct and an acoustic particle velocity node at the top and bottom surfaces of the duct. Initially the flow is not locked and the shedding is broadband. If the leading- and trailing-edge vortex shedding frequency bands overlap the resonance frequency of the duct, the acoustic mode in the duct may be excited. If the flow system is receptive to this frequency, the flow will become locked (through transfer of flow energy to acoustic energy at the resonant frequency) and thus complete a feedback loop, sustaining the resonance. Animations of the excitation of β -mode resonance can be seen in the article by Parker (1997).

Earlier experiments by Welsh and Gibson (1979) found two resonance ranges of $0.10 < St_t < 0.12$ and $0.18 < St_t < 0.21$ for a plate with $c/t = 5$. (Here the Strouhal number, St_t , is based on plate thickness not chord). These different

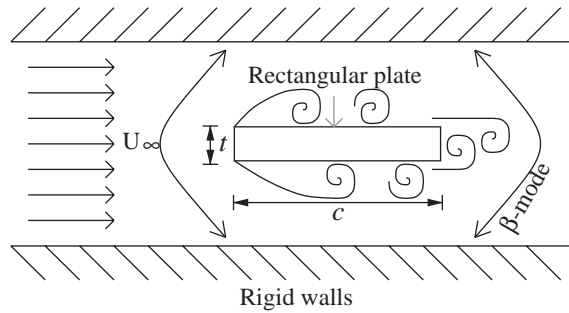


Fig. 1. Schematic of the plate in a duct leading to acoustic resonance.

resonances were excited by slowly increasing the flow velocity until the flow field became locked to the resonant acoustic field. If the plate had an aerodynamic leading edge, there was only one resonant range (Welsh et al., 1984) because there is no leading-edge shedding and the flow at the trailing edge is receptive only over a narrow frequency range. Later experiments by Stokes and Welsh (1986) for plates in the range of $0.5 < c/t < 16$ found that while certain aspect ratios displayed multiple resonant ranges, these also showed a step-wise increase with aspect ratio.

The numerical approach applied to this problem is similar to that used to predict the resonance that occurs in a duct with baffles (Hourigan et al., 1990), and for the resonance generated by a triangular wedge placed at the opening of a resonator tube (Thompson et al., 1992; Hourigan et al., 1993). In those papers a vortex method was employed to model the flow field. The current approach replaces this component with the spectral-element method. With the vortex method, there were difficulties associated with accurately modelling the acoustic energy transfer near boundaries. (Indeed, it was sometimes necessary to artificially truncate the source very close to the boundary). With the current approach, this is not necessary and the acoustic energy transfer can be predicted more accurately and cleanly right up to the boundaries. A minor penalty is that the flow field is calculated at nominally lower Reynolds numbers, however, since the resonance is typically strong for the cases studied and exerts a strong controlling influence on the flow structures responsible for the maintenance of the resonance, we believe the results are applicable to much higher Reynolds numbers as well. This is discussed further below.

2. Numerical technique

The Mach number is assumed to be small, allowing the incompressible flow and acoustic fields to be modelled separately, but with the necessary coupling to enable resonance to be predicted. Specifically, calculation of the flow field supplies the acoustic source field for the acoustic model. It is also important to incorporate the effect of the acoustic field on the flow field since the vortex shedding becomes locked to the acoustic field. To achieve the latter goal, a sinusoidally oscillating cross-flow velocity perturbation is applied at the inlet and side boundaries of the domain for the flow solution. This mimics the resonant β -mode field locally near the plate and controls the vortex shedding from the leading and trailing edges. The actual resonant β -mode in the duct is also calculated by solving an eigenvalue problem. (The field is visualised in Fig. 2 below). Using this time-dependent resonant acoustic field, and the vorticity and velocity field from the flow calculation, the model proposed by Howe (1975, 1980, 1998) is then used to determine the direction of transfer of energy between the acoustic and flow fields. According to the theory, resonance can be sustained if the transfer to the acoustic field is positive. This will be seen to be possible only for certain flow velocities (or equivalently, forcing Strouhal numbers).

2.1. Simulation of the flow field

Simulation of the time-dependent flow field involves solving the incompressible Navier–Stokes equations using the spectral-element method for the spatial discretization and a three-step time-splitting scheme to integrate forward in time. The code has been successfully tested on a number of similar bluff body flows. Details of the method can be found in Tan et al. (1998a–c), Thompson et al. (1996), and Sheard et al. (2003). A careful resolution study was undertaken, by increasing the order of the interpolation polynomials within the spectral elements to ensure the accuracy of velocity predictions throughout the wake was better than 1%. However, while this method allows the flow field to be accurately

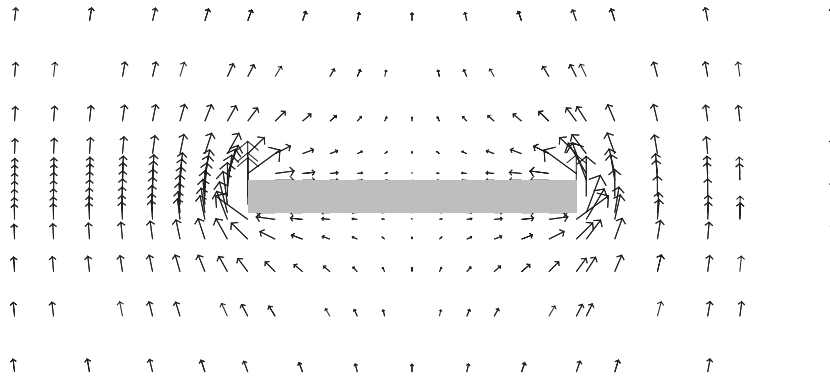


Fig. 2. Plot of the acoustic particle velocity near the plate for $c/t = 10$ at 90° in the acoustic cycle (i.e. maximum in the upward direction).

resolved, the simulations are restricted to a maximum Reynolds number of approximately $Re = 1000$. While experiments are typically at much higher Reynolds number, this restriction is not as important as it first appears. The effect of the acoustic resonance is to strongly control the vortical flow structures, causing them to lock to the flow field, reducing their three-dimensionality and also reducing the formation lengths at the leading and trailing edges of the plate. This means that a two-dimensional flow model performs a reasonable job of capturing the governing flow physics. The Reynolds number chosen for the simulations was $Re = 400$ which is much less than the upper limit of possible Reynolds numbers. This choice was made because, at this Reynolds number, the flow separates and sheds strongly from the leading and trailing edges, and this is approximately the Reynolds number at which the wake undergoes three-dimensional transition. Thus, the two-dimensional model is an accurate representation of the flow at $Re = 400$. At higher Reynolds numbers, restriction to two-dimensional flow leads to a significant and artificial reduction in the wake formation length over a full three-dimensional calculation. Indeed, the predicted Strouhal number for shedding diverges further from the Reynolds number insensitive value measured in experiments. This means that the applicability of predictions to high Reynolds number experiments actually gets worse for higher Reynolds numbers *two-dimensional* simulations.

The effect of the sound field on the flow is taken into account by adding a 2.5% sinusoidal transverse (incompressible) perturbation to the background flow at the inflow and side boundaries of the flow domain. As alluded to previously, this approximates the *compressible* perturbation to the incompressible velocity field near the plate and especially near the corners where the shear layers separate. This is a reasonable approximation because the thickness of the plate is small relative to the wavelength of the acoustic duct mode discussed below. In addition, the most important effect of the acoustic field on the flow field to capture is the locking of the leading- and trailing-edge vortex shedding, which this approach achieves satisfactorily. These duct resonances can be extremely loud (Welsh and Gibson, 1979) reaching levels of up to 120 dB for flow speeds of 15 m s^{-1} , and the size of the perturbation level chosen is consistent with typical resonance amplitudes. It is also similar to the amplitude used by Mills et al. (2002, 2003) in their experimental study using speakers to apply the perturbation. Some simulations were repeated using perturbation amplitudes between 1.25% and 5% to investigate the sensitivity to perturbation level. Only minor qualitative changes resulted from those reported here (Tan, 2000).

The simulation boundaries are placed at $24t$ upstream, $\pm 20t$ in the cross-flow direction and $28t$ downstream of the plate. This results in a blockage of 2.5%, which is close to experimental conditions (between 2.5% and 5.0%) for previous duct resonance studies (Stokes and Welsh, 1986). Thus, the flow domain width is similar to that used in previous experiments. From the experimental point of view, the duct width determines the resonant frequency; however, in the numerical model, the frequency of the acoustic field is imposed on the flow (to evaluate energy transfer) and hence the computational domain size is not an important parameter to match providing it is large enough not to adversely affect the flow near the plate. However, to reiterate, in the computations the frequency is varied to alter the Strouhal number rather than the flow speed, thus maintaining a constant Reynolds number.

2.2. Modelling of the acoustic field

Assuming the flow is in the presence of an external sound field, the theory due to Howe (1975, 1980, 1998) can predict the transfer of power between the flow field and the acoustic field. To sustain the resonance, the time-averaged energy

transfer per cycle needs to be from the flow field to the acoustic field. Although this is a necessary condition, it is not sufficient because the damping in the system may prevent resonance occurring. Therefore these simulations may over predict the range of acoustic resonance.

To perform this analysis, the acoustic power, P , given by the Howe integral specified in Eq. (1) is evaluated on the same grid, using the same spatial spectral discretization scheme as the flow solver.

$$P = -\rho_0 \int \boldsymbol{\omega} \cdot (\mathbf{u} \times \mathbf{v}) \, dV. \tag{1}$$

In this equation, the vorticity $\boldsymbol{\omega}$ and velocity \mathbf{u} are obtained from the flow solver. The remaining terms in the equation are ρ_0 , the mean fluid density, and \mathbf{v} , the acoustic particle velocity. The acoustic particle velocity is found by solving the wave equation [as in Stoneman et al. (1988)]

$$\frac{\partial^2 \Phi}{\partial t^2} = c_s^2 \nabla^2 \Phi, \tag{2}$$

where Φ is the velocity potential and c_s is the sound speed. The components of the gradient of the velocity potential give the acoustic velocity components.

With appropriate boundary conditions, Eq. (2) simulates the fundamental resonant acoustic field in a duct containing a plate. When the velocity potential is separated into the product of a time-dependent and a spatial-dependent component as in Eq. (3), the solution to this system is given by Eqs. (4) and (5):

$$\Phi(x, y, z, t) = \Phi_t(t)\Phi_s(x, y, z), \tag{3}$$

$$\frac{d^2 \Phi_t}{dt^2} + (2\pi f)^2 \Phi_t = 0, \tag{4}$$

$$\nabla^2 \Phi_s + \left(\frac{2\pi f}{c_s}\right)^2 \Phi_s = 0, \tag{5}$$

where f is the acoustic frequency.

The spatial component thus can be calculated by solving an eigenvalue problem. The field is calculated on the same grid as the flow solver using the same spatial discretization scheme. The boundary conditions for the potential are zero normal gradients at the duct walls and at the plate surface. The field is actually only directly calculated in the upper half of the duct. On the centre-line, $\Phi_s = \phi_u$ upstream, and $\Phi_s = \phi_d$ downstream. The exact values of ϕ_u and ϕ_d do not matter since the acoustic potential is only determined to within a scaling factor. These conditions lead to a velocity anti-node on the duct centreline and nodes at the upper and lower duct walls as required by the β -mode. The vector plot in Fig. 2 shows the amplitude and direction of the acoustic particle velocity near a plate with $c/t = 10$. The standing wave oscillates at the same frequency and phase as that of the forcing applied to the flow, since the latter simulates the effect of the acoustic field on the flow in the vicinity of the plate. In the present formulation, both the applied forcing and the acoustic fields can be arbitrarily scaled, and the mean fluid density, ρ_0 , also scales the acoustic power transfer. The amplitude of the acoustic field could be solved, in principle, by solving the fully coupled problem. In this study however, only the direction of energy transfer is considered in determining the possibility of resonance and not the actual magnitude (although relative amplitudes may give some indication of the strength of the resonance). For uniformity in the data set, the amplitude of the acoustic particle velocity is scaled to unity at the centre of the trailing-edge face of the plate and the mean fluid density is set to unity. The scales of velocity and vorticity fields are based on a unit free-stream velocity and a unit plate thickness.

Spatial limits of acoustic power integration

To apply the acoustic model and determine the time-averaged rate of acoustic energy transfer, the integral defined by Eq. (1) needs to be evaluated and time-averaged. Examination of the integrand shows that only regions where vorticity is nonzero can contribute to the acoustic energy transfer. Therefore, a numerical domain of integration that is several plate thicknesses in the upstream and cross-flow direction is sufficient since this captures all the vorticity in the plate boundary layers. In the simulations, the integration boundaries were placed approximately $4t$ and $2t$ from the plate surface in the upstream and cross-flow direction, respectively. The downstream boundary poses a larger challenge because vortices are shed into the wake which extends far downstream because the diffusion and cross-annihilation rates are low. The method used to overcome this problem is described next.

The time-averaged sources/sinks of acoustic power are located in regions near the plate. The vortices further downstream do not contribute any net power because the amount of energy generated in one half of an acoustic cycle is effectively negated in the other. This is also the reason why an arbitrarily placed downstream limit will cause a bias. As

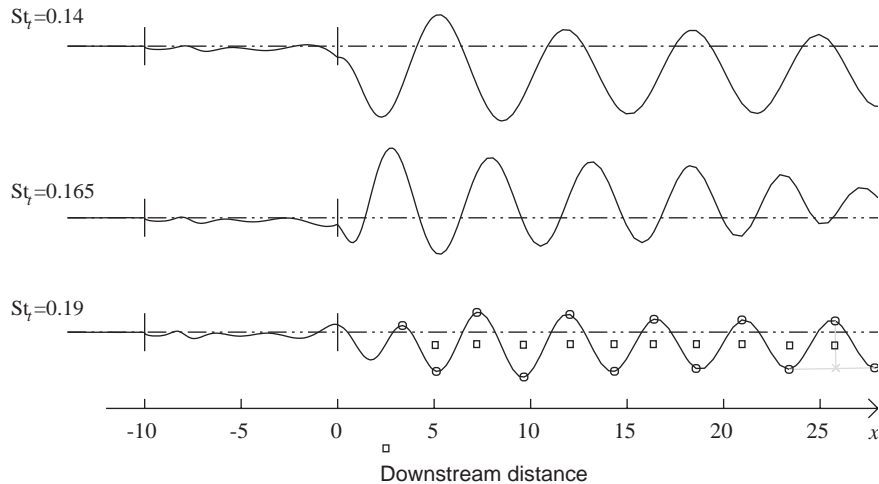


Fig. 3. Time-averaged energy transfer per cycle determined for different downstream locations (x) of the computational boundary. The aspect ratio is $c/t = 10$ and $St_t = 0.14, 0.165$ and 0.19 . Vertical lines represent the leading and trailing edge of the plate and the dotted lines indicate the zero value. See text for further details.

the vortices convect downstream and cross this artificial boundary, they contribute to the average acoustic power for only the part of a cycle before crossing the boundary and exiting the domain. An accurate estimate of the time-averaged acoustic energy transfer must have this bias removed.

This is done by first calculating the time-averaged acoustic power transfer for various downstream locations of the integration boundary. The cumulative sum in the downstream direction of the acoustic power generated is shown for a selection of Strouhal numbers for $c/t = 10$ in Fig. 3. From these plots, it is clear that downstream of the trailing-edge shedding region, the power trace in the wake oscillates about a time-averaged value; this mean is established in the region immediately downstream of the trailing edge of the plate. The mean acoustic power generated is estimated in each downstream cycle (shown by the boxes) by averaging amplitudes at consecutive peaks or troughs and then averaging those values with the value at the intermediate troughs or peaks. This is shown diagrammatically by the gray lines in the lower plot of Fig. 3. This effectively gives the local time-mean value of the oscillating signal. As will be seen by the error bars in Fig. 4, the error in estimating the mean between each downstream cycle is small relative to the overall variation in power transfer.

3. Results

The time-averaged acoustic power transfer is calculated for plates with aspect ratios between $6 \leq c/t \leq 16$. The analysis is performed only within the range of duct (forcing) frequencies that result in locked flow for this level of forcing. (In experiments, the duct resonance frequency is generally fixed and the Strouhal number is varied by changing the inflow velocity; however, this is equivalent to fixing the inflow velocity and varying the acoustic frequency. This latter approach is more convenient computationally.) Fig. 4 shows the predicted values of the time-averaged acoustic energy transfer from the flow field to the acoustic field. Duct acoustic resonance can only be sustained when the values are positive. Note that many aspect ratios show multiple frequency ranges for which resonance is possible. In addition, as the aspect ratio is increased, the frequencies at which resonance occurs also decrease as shown by the dashed lines in Fig. 4. As this occurs, another resonance range develops at a higher frequency and follows the same trend.

A simplified way to view this behaviour is to plot the resonance range (based on chord) of the dominant frequency as a function of aspect ratio as in Fig. 5. The frequency range where resonance can occur clearly shows a stepwise increase with aspect ratio. The simulations predict that the steps are approximately $St_c = 0.55n$, for integer n . The results from Stokes and Welsh (1986) are also plotted for comparison. Although both simulations and experimental results show a similar stepwise variation, the size of the step is slightly higher for the experiments (approximately $St_c = 0.6n$). This is presumably due to the much higher Reynolds numbers used for the experiments leading to a slightly larger effective

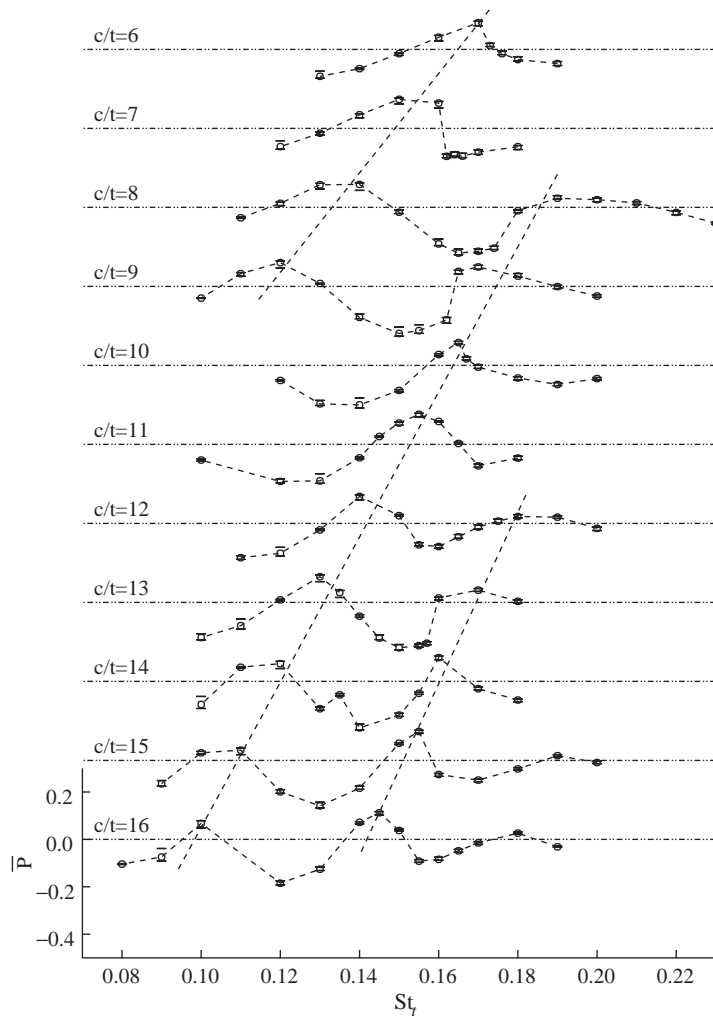


Fig. 4. Time-averaged energy transfer per cycle from the flow field to the sound field for plates with aspect ratios between $c/t = 6$ and 16 as a function of Strouhal number.

convection velocity of the vortices. Note that the difference between the Strouhal numbers steps is directly related to the mean convection velocity of vortices along the upper and lower faces of the plate. Given an average convection velocity U_c , and that there are n vortices distributed along the plate, the shedding frequency is $f = nU_c/c$. Substituting this into the Strouhal number definition gives $St_c = fc/U_\infty = nU_c/U_\infty$. The numerical results therefore give $U_c = 0.55U_\infty$.

This stepping is also seen in other related flow-acoustic problems. For instance, Fig. 6.3.4 from Howe (1998) shows similar experimental Strouhal number stepping for a jet–edge interaction problem, which is influenced by a similar feedback mechanism.

To further understand the frequency selection of the resonance process, identification of the main source/sink regions of the acoustic power was undertaken. To achieve this, the results of varying the downstream integration limit presented in Fig. 3 is revisited. To remove the fluctuations due to the pairs of vortices further downstream, a running-average is taken with an averaging length approximately the distance between a pair of like-signed wake vortices. The result of this process is shown in Fig. 6 for the cases with $c/t = 10$, and $St_t = 0.14, 0.165$ and 0.19 . In each case, the values are approximately constant upstream of the trailing edge and further downstream. This means that there is no significant (time-averaged) power being generated in these regions. The large variation occurs just downstream of the trailing edge. This shows that there is a large sink/source depending on Strouhal number for this region. Analysis of numerous other cases of different chord to thickness ratios and Strouhal numbers also show the main source/sink is in the region just downstream of the trailing edge.

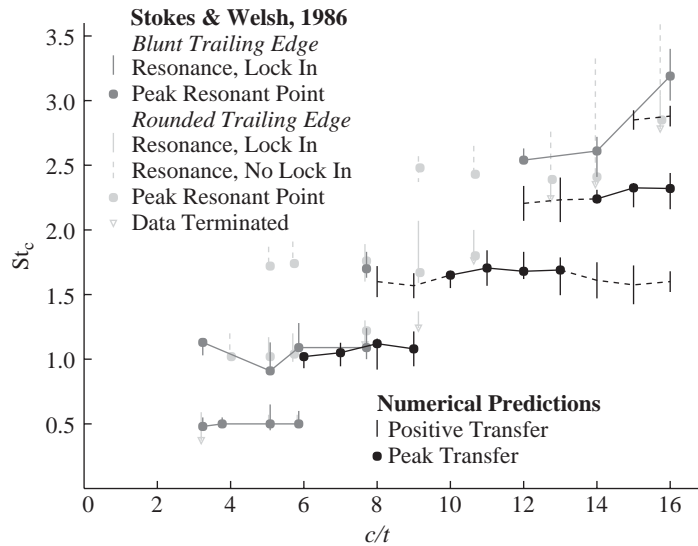


Fig. 5. Strouhal number St_c ranges for which positive transfer of energy between the flow and the sound field occurs. The experimental results of Stokes and Welsh (1986) are denoted by the grey circles and lines as listed in the legend. The numerical predictions are given by the black circles and lines.

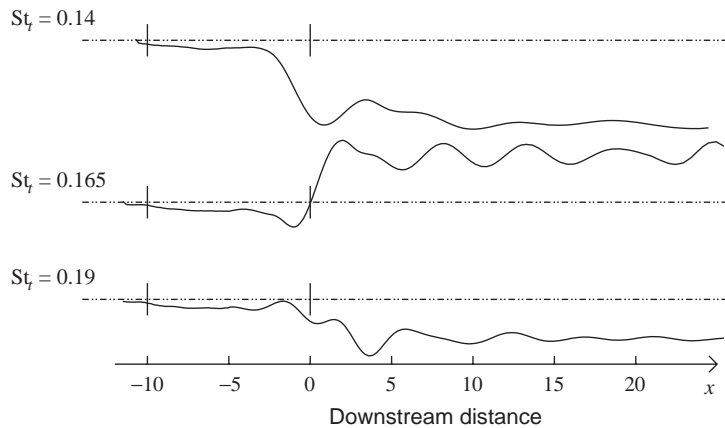


Fig. 6. A running average of the cumulative sum in the downstream direction of the time-averaged acoustic power for $c/t = 10$. The Strouhal numbers are $St_t = 0.14, 0.165$ and 0.19 . The running average is taken over approximately one hydrodynamic wavelength of the oscillations downstream of the plate, i.e., the distance between two like-signed vortices in the wake.

The reason for the region just downstream of the trailing edge being the only prominent net contributor of acoustic power can be easily related to the velocity and vorticity fields of the flow. In the regions away from the plate in the upstream and cross-stream direction, vorticity is negligible and therefore so is the energy transfer. The regions near the top and bottom surface which contain vorticity from the leading-edge shedding and the boundary layer are not significant sources of acoustic power because the acoustic particle velocity is approximately parallel to the flow velocity; according to the Howe integral, this condition leads to little acoustic power generation. As mentioned earlier, the vortices downstream of the plate have no net contribution because any energy generated in one half of a cycle is absorbed in the other. In the region just downstream of the plate, acoustic power generation is high because of the presence of vorticity from leading and trailing-edge shedding which can lead to energy transfer because the flow and acoustic fields are almost perpendicular at this location. Unlike regions further downstream, this region has a net contribution because of the presence of the plate. To better understand this, consider the vorticity immediately

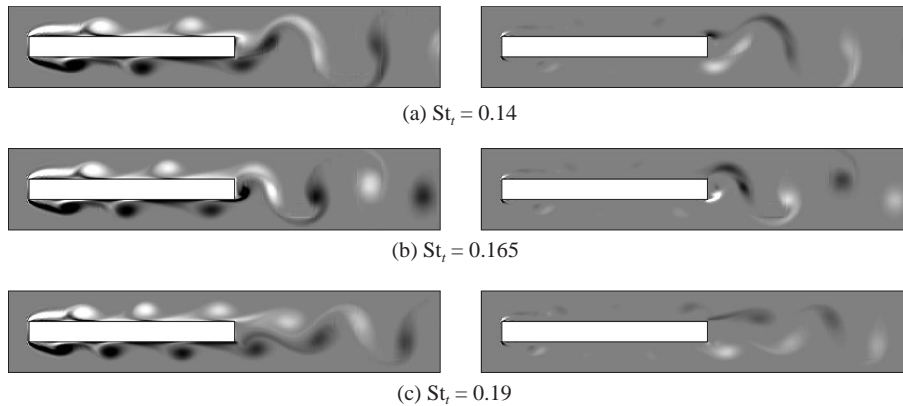


Fig. 7. Plots of vorticity in the left column and instantaneous acoustic power on the right column taken at 90° in the acoustic cycle for cases with $c/t = 10$ and (a) $St_t = 0.14$, (b) $St_t = 0.165$, and (c) $St_t = 0.19$. Positive/negative regions are represented by the darker/lighter shades. The greyscale ranged from $+/- 0.2$ to $+/- 4.0$ with maximum/minimum intensity for larger magnitudes.

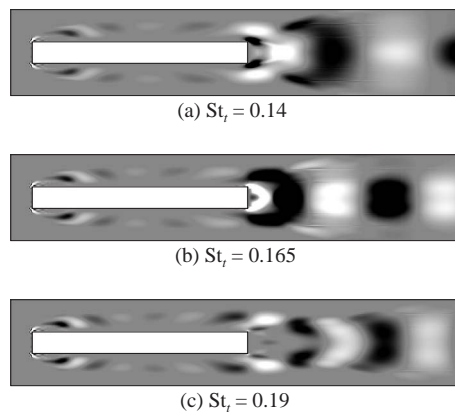


Fig. 8. Time-averaged acoustic power for cases with $c/t = 10$ and (a) $St_t = 0.14$, (b) $St_t = 0.165$, and (c) $St_t = 0.19$.

upstream of the trailing edge and that forming into a nascent vortex structure from shedding from the trailing edge into the wake, in one half of an acoustic cycle. This forms into a wake vortex structure and begins to convect downstream in the next half cycle. In the first half of the cycle, the acoustic power generated is relatively small because the vortex is not fully formed and is moving only relatively slowly, but in the second half of the cycle, a significant amount of acoustic power is generated or absorbed. This results in a net generation/absorption of acoustic energy over a cycle.

Some visualizations will now be presented to elucidate the frequency selection process for resonance to exist. Fig. 7 shows the vorticity and instantaneous acoustic power intensity taken at 90° in the acoustic (forcing) cycle when the acoustic particle velocity (perturbation) is maximum in the upward direction. The cases shown are again for $c/t = 10$ and $St_t = 0.14$, 0.165 and 0.19 . The acoustic power intensity is obtained by calculating the instantaneous value of the integrand on the right hand side of Eq. (1). Fig. 8 shows the time-averaged acoustic power intensity for the same cases. At a duct frequency of $St_t = 0.14$, resonance could not be sustained because the net transfer of energy is from the acoustic field to the flow field. The opposite occurs at $St_t = 0.165$ and the system could sustain an acoustic resonance. Resonance is no longer possible when the duct frequency is increased to $St_t = 0.19$.

As shown earlier, the main source of acoustic power is from the region just downstream of the plate. The main difference between these flows is the phase of the vortices entering the region just downstream of the trailing edge. The case where there is a positive transfer of acoustic power from the flow field to the acoustic field will first be considered (i.e. $St_t = 0.165$). At 90° in the cycle, negative (clockwise) vorticity from the top side of the plate is dominant in this region. As shown by the top left sketch in Fig. 9, with the acoustic particle velocity in the upward direction, negative

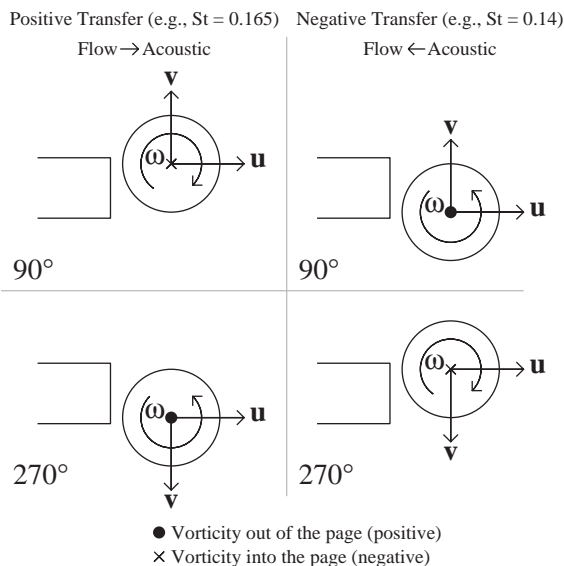


Fig. 9. A schematic diagram showing the direction of acoustic power transfer from vortices near the trailing edge based on the integrand of Eq. (1).

vorticity in the vortex structure and given that the flow is predominantly in the streamwise direction, the model predicts a positive transfer of energy to the acoustic field. This is confirmed by the positive region just downstream of the plate as shown by the acoustic power intensity plot in Fig. 7. Positive (anti-clockwise) vorticity from the bottom of the plate will be dominant in this region in the second half of the cycle (270°). As shown in the lower left sketch of Fig. 9, now the acoustic particle velocity is in the downward direction and this again results in positive transfer of energy to the acoustic field. Thus, over an entire cycle, this situation leads to the time-averaged positive energy transfer from this region as shown in Fig. 8. Therefore, resonance can be sustained in this case because of the positive contribution from this region which dominates the overall balance.

In the other two cases, $St_r = 0.14$ and 0.19 , Fig. 7 shows positive (anti-clockwise) vorticity from the bottom of the plate is dominant in this region at 90° in the cycle. In the other half of the cycle, negative (clockwise) vorticity would be present and both of these cases are represented by the idealized sketches in the right hand column of Fig. 9. This is confirmed by the regions of negative instantaneous power transfer shown in Fig. 7, and the mean acoustic power transfer plots in Fig. 8.

4. Discussion

It is now possible to relate the resonance ranges discussed earlier with the flow dynamics. With the flow locked to the sound (forcing) field, the leading-edge shedding is phase-locked to the forcing and sheds a pair of vortices each period. The convection velocity of these vortices is relatively independent of forcing frequency and amplitude (Tan et al., 1998a, b). Trailing-edge vortices are shed between the passing of leading-edge vortices at the trailing edge. As discussed earlier, the direction of acoustic power transfer is governed by the phase as the vortices enter the region just downstream of the trailing edge. For a fixed aspect ratio, increasing the forcing frequency would retard the phase in the acoustic (forcing) cycle at which the leading-edge vortices pass the trailing edge. It is then possible to observe multiple frequency bands where resonance is possible if the flow still locks to that frequency. Each of these resonance ranges would be one full cycle apart associated with either an increment or decrement in the number of vortices along the upper and lower faces of the plate. If the plate length is increased, it would take more time for the vortices to traverse the plate and therefore the relative phase at the trailing edge would be retarded if the forcing frequency is fixed. To compensate for this, the forcing frequency would have to be reduced to maintain the relative phase favourable for resonance as observed in Fig. 4.

The relationship between the aspect ratio and the forcing frequency is evident in Fig. 5. The stepwise increase in frequency (St_c) range where the system resonates is such that the flow maintains this favourable phase. The reason for

this stepping is similar to the frequency selection in the natural shedding case and forced shedding case as described in the introduction. In all three cases, the stepping in frequency is related to maintaining a constant phase between the leading-edge shedding or forcing (which is equivalent because the shed vortices are phase-locked), and the arrival of these vortices at the trailing edge. These conclusions are consistent with those found in the experimental work of Mills et al. (2002, 2003) on forced flows past plates.

The vorticity plots in Fig. 7 show the strongest base shedding at $St_t = 0.165$ where resonance is possible. This case also corresponds to a strong mean base suction. Strong trailing-edge vortex shedding has also been associated with high sound pressure levels in duct resonance cases and base pressure measurements (Mills et al., 2002, 2003). As the duct frequency is increased ($St_t = 0.19$), the trailing-edge shedding weakens and there is a drop in base suction (Tan et al., 1998a–c). These simulations predict that resonance is still possible in cases where base shedding is suppressed. This is normally associated with the higher frequency band for plates with multiple resonance bands. In these cases, resonance is sustained primarily by the leading-edge vortices which pass the trailing edge and enter the wake at a favourable time in the cycle instead of the combined leading- and trailing-edge vortices shown in Fig. 7(b).

The plots of mean acoustic power transfer in Fig. 8 show regions of sources and sinks downstream of the plate. As discussed earlier, the main source/sink of net acoustic power is from the region just downstream of the plate. Further downstream, the pairs of sources and sinks negate each other. However, from the Howe integral (Eq. (1)), altering the direction of the acoustic particle velocity from the cross-flow direction toward the free-stream direction in a local region can significantly reduce a source or sink. This presents means to exert some control over the development of resonance. Experiments by Stoneman et al. (1988) achieved this aim by placing a small plate in the wake. In those experiments, by varying the downstream position of the small plate, it was possible to control when resonance was excited.

5. Conclusions

The coupled flow and acoustic model presented in this paper is able to predict the Strouhal number ranges over which resonance may occur in good agreement with experimental observations. Furthermore, using the aeroacoustic theory of Howe (1998), the simulations have allowed identification of the acoustic source and sink regions in the flow. The main source/sink of acoustic energy occurs in the region immediately downstream of the trailing edge and is associated with wake vortices forming and convecting in synchronization with leading-edge vortices passing the trailing edge. The crucial element in sustaining acoustic resonance is the relative phase between the vortices entering the wake and the acoustic (forcing) field. This results in the Strouhal number ranges for which resonance occurs displaying a stepwise increase with aspect ratio as observed experimentally.

Acknowledgements

The authors wish to acknowledge financial and computing support from the Victorian Partnership for Advanced Computing (VPAC) and the Australian Partnership for Advanced Computing (APAC).

References

- Curle, N., 1955. The influence of solid boundaries on aerodynamic sound. *Proceedings of the Royal Society of London A* 231, 505–514.
- Hardin, J.C., Pope, D.S., 1994. An acoustic/viscous splitting technique for computational aeroacoustics. *Theoretical and Computational Fluid Dynamics* 6, 323–340.
- Hourigan, K., Welsh, M.C., Thompson, M.C., Stokes, A.N., 1990. Aerodynamic sources of acoustic resonance in a duct with baffles. *Journal of Fluids and Structures* 4, 345–370.
- Hourigan, K., Thompson, M.C., Brocher, E., Andrianantoandro, A., 1993. Coupling of vortex shedding with the fundamental resonant mode of a resonator tube. *Noise Control Engineering Journal* 41 (2), 331–338.
- Hourigan, K., Thompson, M.C., Tan, B.T., 2001. Self-sustained oscillations in flows around long blunt plates. *Journal of Fluids and Structures* 15 (3/4), 387–398.
- Howe, M.S., 1975. Contributions to the theory of aerodynamic sound, with applications to excess jet noise and the theory of the flute. *Journal of Fluid Mechanics* 71, 625–673.
- Howe, M.S., 1980. The dissipation of sound at an edge. *Journal of Sound and Vibrations* 70, 407–411.
- Howe, M.S., 1998. *Acoustics of Fluid–Structure Interactions*. Cambridge Monographs on Mechanics. Cambridge University Press, Cambridge, U.K.

- Inoue, O., Hatakeyama, N., 2002. Sound generated by a two-dimensional circular cylinder in a uniform flow. *Journal of Fluid Mechanics* 471, 285–314.
- Lele, S.K., 1997. Computational aeroacoustics: a review. AIAA Paper 97-0018.
- Lighthill, M.J., 1952. On sound generated aerodynamically: I. General theory. *Proceedings of the Royal Society of London A* 221, 564–587.
- Mills, R., Sheridan, J., Hourigan, K., 2002. Response of base suction and vortex shedding from rectangular prisms. *Journal of Fluid Mechanics* 461, 25–49.
- Mills, R., Sheridan, J., Hourigan, K., 2003. Particle image velocimetry and flow visualization of flow around rectangular cylinders. *Journal of Fluid Mechanics* 478, 299–323.
- Moin, P., Mahesh, K., 1998. Direct numerical simulation: a tool in turbulence research. *Annual Reviews of Fluid Mechanics* 30, 539–564.
- Nakamura, Y., Ohya, Y., Tsuruta, H., 1991. Experiments on vortex shedding from flat plates with square leading and trailing edges. *Journal of Fluid Mechanics* 222, 437–447.
- Nakayama, R., Nakamura, Y., Ohya, Y., Ozono, S., 1993. A numerical study of the flow around flat plates at low Reynolds numbers. *Journal of Wind Engineering and Industrial Aerodynamics* 46 & 47, 255–264.
- Naudascher, E., Wang, Y., 1993. Flow-induced vibration of prismatic bodies and grids of prisms. *Journal of Fluids and Structures* 7, 341–373.
- Ohya, Y., Nakamura, Y., Ozono, S., Tsuruta, H., Nakayama, R., 1992. A numerical study of vortex shedding from flat plates with square leading and trailing edges. *Journal of Fluid Mechanics* 236, 445–460.
- Parker, R., 1966. Resonant effects in wake shedding from parallel plates: some experimental observations. *Journal of Sound and Vibrations* 4, 62–72.
- Parker, R., 1997. Aeroacoustics. *International Journal of Fluid Dynamics* (<http://elecpress.monash.edu.au/ijfd>) 1, Article 1.
- Sheard, G.J., Thompson, M.C., Hourigan, K., 2003. From spheres to circular cylinders: classification of bluff ring transitions and structure of bluff ring wakes. *Journal of Fluid Mechanics* 492, 147–180.
- Shen, W.Z., Sorensen, J.N., 1999. Comment on the aeroacoustic formulation of Hardin and Pope. *AIAA Journal* 37 (1), 141–143.
- Stokes, A.N., Welsh, M.C., 1986. Sound interaction in a duct containing a plate, Part II: square leading edge. *Journal of Sound and Vibrations* 104 (1), 55–73.
- Stoneman, S.A.T., Hourigan, K., Stokes, A.N., Welsh, M.C., 1988. Resonant sound caused by flow past two plates in tandem in a duct. *Journal of Fluid Mechanics* 192, 455–484.
- Tam, C.K.W., 1995. Computational aeroacoustics: issues and methods. *AIAA Journal* 33, 1788–1796.
- Tam, C.K.W., Hardin, J.C., 1997. Proceedings of the second computational aeroacoustics workshop (CAA) on benchmark problems. NASA CP-3352.
- Tan, B.T., 2000. Vortex shedding and interactions in flow around Bluff plates. Ph.D. Thesis, Department of Mechanical Engineering, Monash University.
- Tan, B.T., Thompson, M.C., Hourigan, K., 1998a. Simulated flow around long rectangular plates under cross-flow perturbations. *International Journal of Fluid Dynamics* (<http://elecpress.monash.edu.au/ijfd>) 2, Article 1.
- Tan, B.T., Thompson, M.C., Hourigan, K., 1998b. Simulation of perturbed flow around a rectangular cylinder. Proceedings of the ASME Fluids Engineering Division Summer Meeting, published on CDROM, Paper No. FEDSM98-5166.
- Tan, B.T., Thompson, M.C., Hourigan, K., 1998c. Numerical predictions of forces on a long rectangular plate subjected to cross-flow perturbation. Proceedings of the 13th Australasian Fluid Mechanics Conference, Monash University, Melbourne, Australia. pp. 789–794.
- Thompson, M.C., Hourigan, K., Welsh, M.C., Brocher, E., 1992. Acoustic sources in a tripped flow past a resonator tube. *AIAA Journal* 30 (2), 1484–1491.
- Thompson, M.C., Hourigan, K., Sheridan, J., 1996. Three-dimensional instabilities in the wake of a circular cylinder. *Experimental Thermal Fluid Science* 12, 190–196.
- Welsh, M.C., Gibson, D.C., 1979. Interaction of induced sound with flow past a square leading-edged plate in a duct. *Journal of Sound and Vibrations* 67 (4), 501–511.
- Welsh, M.C., Stokes, A.N., Parker, R., 1984. Flow-resonant sound interaction in a duct containing a plate, Part I: semi-circular leading edge. *Journal of Sound and Vibrations* 95 (3), 305–323.